Nano mechanical study on a single layer TiC/TI6AI4V-ELI composite manufactured with laser metal deposition

Pushetso Ramasobane[11], *Madindwa Peter* Mashinini[1], and *Bathusile Nelisiwe* Masina[1,2]

[1]* Department of Mechanical and Industrial Engineering Technology,University of Johannesburg, Johannesburg 2094, South Africa
[2] Photonics, Manufacturing Cluster, Council for Scientific and Industrial Research, Meiring Naude, Brummeria Pretoria 0001, South Africa

Abstract. This study investigated the nano mechanical properties of Ti6Al4V-ELI embraced with TiC particles, synthesized with in situ laser metal deposition technique. The 3.85% feed ratio fraction TiC/Ti6Al4V-ELI composite samples were manufactured at four varying energy densities. The beta grain boundary and the acicular alpha primary matrix were found to have diverse morphologies of carbide particles due to the in-situ reaction. The effect of energy density is observed on the microstructure and nano mechanical properties. An average off set of 650 nm was recorded after the nano-indentation in the matrix at a maximum load of 400 mN

1 Corresponding author: pushetso@icloud.com

1 Introduction

Laser metal deposition (LMD), which offers exceptional design flexibility and quick lead times, has grown in popularity recently due to its many advantages [1]. LMD is a sophisticated process that is affected by a wide range of process variables, including powder flow feed rate, laser power, and scanning speed. The titanium matrix composite (TMC) may be fabricated with greater flexibility due to the LMD process. LMD has been utilized to fabricate clad that has a composite matrix or improved material. Additionally, according to the research [2–4], the material with the best attributes is only partially melted to preserve those physical characteristics.

When compared to conventional surface modification techniques, LMD offers the benefits of minimized preparation times, sound quality, and excellent interface combinations including the prevention of fractures brought on by high - temperature impacts [5–6]. A Ti/7YSZ composite clad made with the LMD technique, as developed by Cui et al., refined the wear resistance of the TC4 titanium alloy [7]. The study suggests that at different laser scanning speeds, the microstructure of the Ti-based composite surface treatment cladding system changed from top to bottom [7]. TiC/Ti6Al4V composites with different Y element concentrations were created by Wang et al. [8]. Studying the effect of Y content on the microstructure and mechanical characteristics of composites revealed some interesting results [8], but the new material's integrity and matrix interaction were both poor. The strengthening phase produced by the in-situ reaction approach, on the other hand, was refined and steadier and more had a strong connection to the matrix [9]. This strategy has drawn a lot of interest consequently [9]. Using a mixed powder of C and Si and the laser nitriding technique, LMD was also utilized to manufacture Ti/SiC and in-situ TiN dendrite-strengthened composite coatings on a Ti6Al4V substrate [10–11]. Even so, research on LMD of TiC/Ti6Al4V composites with completely melted TiC is few.

Ramasobane et al. [12], studied the influence of ED on the microstructure of TiC/Ti6Al4V-ELI and reported that overlap zones showed lower hardness reading. To further understand this behavior nano-indentation studies is proposed to further investigate the behavior of phases previously reported on in literature [12]. Titanium matrix composites such as TiC/Ti6Al4V-ELI are able to meet the heightened requirements of quickly developing high-tech industries including aviation, aerospace, electronics, and automotive, hence expanding their engineering applications in particular.

In this work, a 3.85 % TiC volume ratio fraction to Ti6Al4V-ELI was achieved by in situ fabrication of TiC/Ti6Al4V-ELI utilizing LMD techniques at four different energy densities (EDs). The overlap zones are further characterized with scanning electron microscope equipped with electron dispersive spectroscopy (SEM/EDS) and nano-indentation. The grain growth in the overlap zones are studied. Also highlighted is how carbide particles affect the nano-mechanical characteristics of TiC/Ti6Al4V-ELI.

2 Experimental Procedure

2.1 Materials

The matrix was provided by TLS Technik GMbH & Co, Bitterfeld, Germany, and consisted of a grade 23, pre-alloyed Ti6Al4V ELI powder that was spherical with a particle size distribution between 45 and 100 μm. As a reinforcing material, Stanford Advance Material

provided a TiC powder with particle size in the range of -140+325 mesh. Fig. 1 displays the morphologies of the TiC and Ti6Al4V-ELI powders.

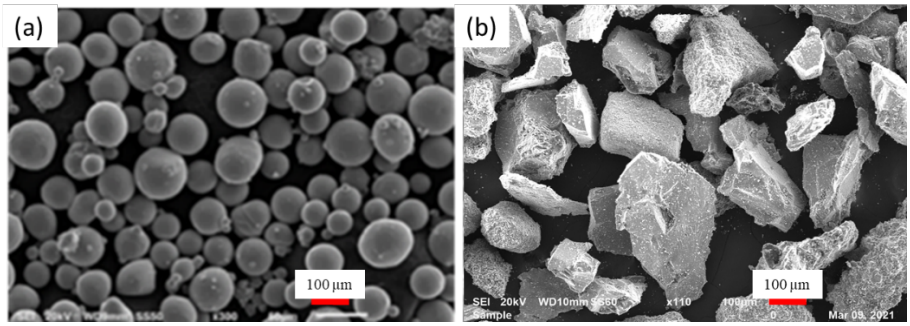

Fig. 1: SEM images of the powders (a) Ti6Al4V-ELI, (b) TiC [12].

As demonstrated in Fig. 1, the Ti6Al4V-ELI revealed spherical, smooth, and porosity-free particles (a). In additional research [12–13], spherically formed and smooth Ti6Al4V ELI particles were observed. However, the TiC powder in Fig. 1(b) showed coarse, irregular-shaped particles. TiC particles with odd shapes have also been documented in the literature [13]. The substrate, a Ti6Al4V base plate that had been washed in acetone, was utilized to place the samples on.

2.2 Methods

All samples were fabricated using a KUKA robot, a 3-way nozzle, and an IPG fiber laser (1073 nm wavelength) processing equipment. The Ti6Al4V-ELI and TiC powders were conveyed by gas during deposition using a GTV powder network (D-57629), which was outfitted with two powder feed hoppers. For Ti6Al4V-ELI, the powder flow rate was set at 5.0 rpm, while for TiC, it was set at 0.3 rpm. During the deposition procedure, the powder carrier gas was blasted at a rate of 1.5 l/min. To prevent oxidation on the created samples, argon gas was employed as a shielding gas. For each deposition, energy density of 90, 96, 102 and 108 J/mm^2 was utilized. During sample deposition, the following process parameters were kept constant: a beam diameter of 2 mm, a gas flow rate of 12 l/min, and a scanning speed of 0.5 m/min. Sandblasting was used to get the Ti6Al4V base plate ready for depositing. With 50%-layer (thickness 231.5 µm) overlap in the y-direction, long single-line tracks of around 40 mm were deposited. A LMD schematic is shown in Fig. 2 below.

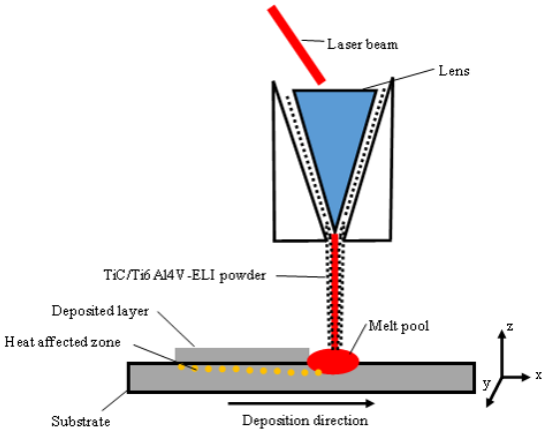

Fig. 2: Schematic diagram of LMD [12].

Standard metallurgical practice for metallographic sample preparations were followed. The Anton Paar nano-indentation device was used to measure nano-indentation. A Berkovich indenter with a diameter of 150 nm was used for all measurements, with a maximum applied force of 400 mN. Three nano-indentation patterns fig. 3 were measured for each sample, and the average was taken as the material's nano-properties.

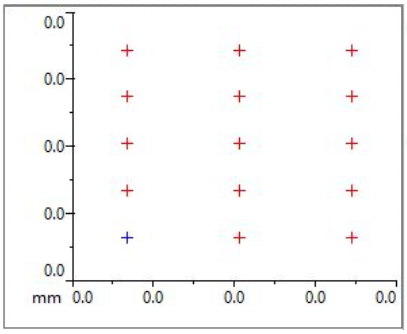

Fig. 3. Nano-indent formation

3 Results and Discussions

3.1 Microstructure

TiC/Ti6Al4V-ELI samples were observed on the SEM and the following observation were made long chains and dendritic particles along the grain boundary of the composite, shown in fig. 4(a). Carbide veins are observed with eutectic granular morphology. Fig. 4(b) shows chain shape morphology of carbides along columnar grains, and granular eutectic in the matrix. Fig. 4 (a) and (b), shows the energy density (ED) of 90 and 96 J/mm^2. Same trends of carbide morphologies are observed. Similar carbides morphologies were reported by Li, et al. [13]. Fig 4(c) and (d), shows microstructure morphologies of samples fabricated at higher ED of 102 and 108 J/mm^2. Granular eutectic carbides are observed imbedded on the matrix in sample 4(c) and (d). carbide veins or chains are observed in fig 4(c). clustered regions of carbides are observed in fig. 4(d). prior beta grains are observed in the matrix along with the chain carbide. The formation of chain and granular eutectic carbides can be attributed to high temperature during solidification. In-situ alloying of TiC and Ti6Al4V-ELI

shows good interfacial bonding, as observed in fig. 4. From the observed carbides morphology, it is evident that ED above 100 J/mm^2 result in chain and granular eutectic carbides, in TiC/Ti6Al4V-ELI composite, when fabricated with LMD technique.

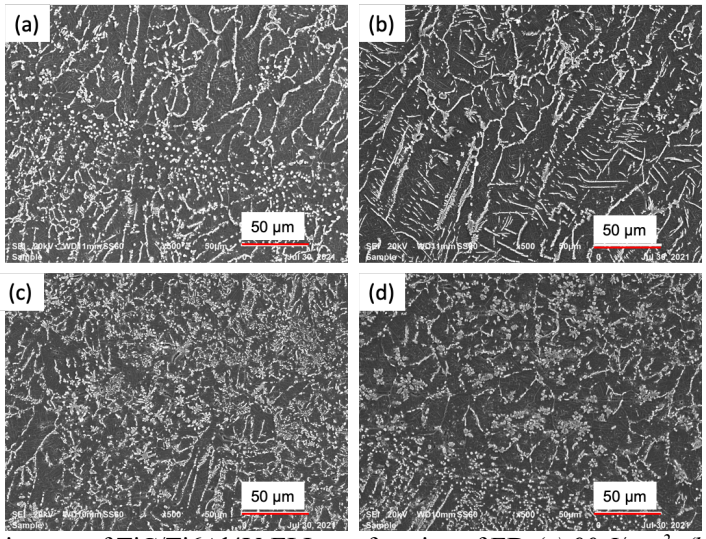

Fig. 4: SEM images of TiC/Ti6Al4V-ELI as a function of ED *(a) 90 J/mm^2, (b) 96 J/mm^2, (c) 102 J/mm^2 and (c)* 108 J/mm^2

3.2 Nano-indentation

Fig.5 below shows the nano indentation plots of load vs penetration depth of a 3.85% TiC feed ratio to Ti6Al4V-ELI, obtained on the overlap zones. The analysis of these process is based on the Oliver-Pharr method, which involves recording of load-displacement curve as the indenter penetrates the material. From the fig. 5, it is observed that multiple yields points are achieved at 200 mN, 300 -400 mN corresponding to the depth of 1100, 1200 and at 1300 nm. This multiple yields points indicates that the composite experiences deformation.

In fig. 5(a) nano-indentation plot shows similar trend for across ED. The indentation on the matrix of the of TiC/Ti6Al4V-ELI composite, shows that an offset of 1400 nm, occurred at a load of 400m N, for all the EDs, this is shown in fig 5. ED has no significant effect on the matrix of TiC/Ti6Al4V-ELI. The nano-mechanical properties are summed up in table 1, below. Where H_{IT}, E_{IT} and E_r are indentation hardness, indentation modulus of elasticity and effective modulus of elasticity (GPa), respectively.

Table 1: nano mechanical properties of the matrix grain

ED (J/mm^2)	H_{IT} (MPa)	E_{IT} (GPa)	E_r
90	64972,95	635,8	409,54
96	66909,2	638,17	402,15
102	51231	449,95	331,36
108	28156,23	368,49	290,61

In fig. 5(b) it is observed that ED of 90-96 J/mm^2, they follow the similar trend and reaches a maximum penetration depth of 1400 nm at a load of 400 mN and an offset of 600 nm was

recorded. ED of 102 – 106 J/mm^2 on the composite shows that penetration depth of 1500nm, was achieved at load lower than 200 mN, and an offset of 700 nm was recorded. An off set of 600 nm. The nano-mechanical properties are summed up in table 2, below.

Table 2: nano mechanical properties of the composite (interface) grain

ED (J/mm^2)	H_{IT} (MPa)	E_{IT} (GPa)	E_r (GPa)
90	61361	601,9	391,39
96	30105,08	352,92	279,17
102	32193,71	421,96	312,41
108	37218,55	363,89	286,55

Fig. 5(c), shows the nano-indentation plots of carbide phases, an offset of 600 nm for ED of 90 – 96 J/mm^2 after loading at a maximum of 400 mN. ED of 102 – 108 J/mm^2 shows that penetration depth of 1500 nm was achieved at a load of 100 mN. This shows that ED of 102 – 108 J/mm^2 have a direct effect on the ductility of TiC/Ti6Al4V-ELI. The nano-mechanical properties are summed up in table 3, below.

Table 3: nano mechanical properties of the carbide grain

ED (J/mm^2)	H_{IT} (MPa)	E_{IT} (GPa)	E_r (GPa)
90	175250	1965,72	707,57
96	183273,67	1992,1	711,9
102	75070	992,82	539,35
108	65553,87	603,91	404.6

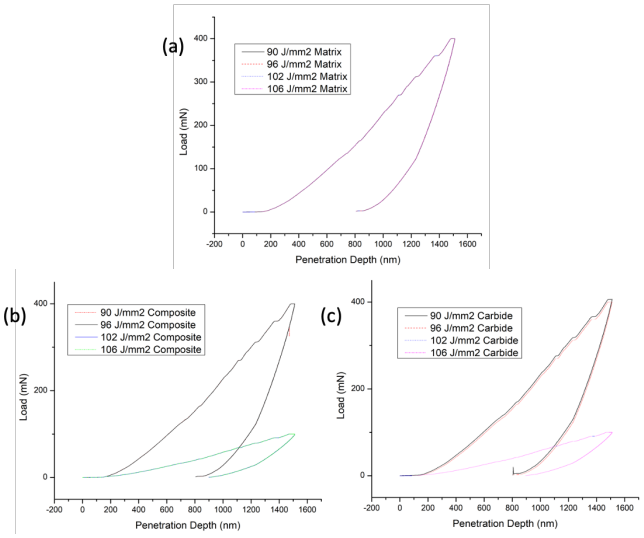

Fig. 5: Nano-indentation plot of TiC/Ti6Al4V-ELI (a) Matrix grain, (b) Composite grain and (c) Carbide grain

4 Conclusion

In this work, the in-situ reaction of Ti6Al4V-ELI and TiC powders produced a TiC/Ti6Al4V-ELI composite using the LMD method. It was clear how energy density

affected the emergence of microstructures and nanomechanical systems. The following findings were reached:

- LMD of Ti6Al4V-ELI and TiC result in the formation of carbide precipitates of various morphologies.
- Energy density is directly proportional to the effective modulus of elasticity.
- indentation modulus decreases with increasing energy density.

Acknowledgement

The Department of Science and Innovation (DSI) is thanked for funding through the Collaborative Program in Additive manufacturing (CPAM). The Council for Scientific and Industrial Research is thanked for laboratory equipment support.

References

[1] J. Kranz, D. Hertzog and C. Emmelmann, J. Laser Appl. **27,** (2015)

[2] L. Li, J. Wang, P. Lin and H. Liu, Ceram. Int. **43**, (2017)

[3] N. K. K. Arthur, C. Siyaya, S. Pityana and M. Tlotleng, J. Mater. Eng. Perform. **30**, (2021)

[4] J. Qi, H. Wang, C. M. Zou and Z. J. Wei, Mater. Sci. Eng. A, **553,** (2012)

[5] F. Weng, H. Yu, C. Chen, J. Liu and L. Zhao, J. of Alloys Compd., **650**, (2015)

[6] Q. Meng, L. Geng and D. Ni, Mater. Lett., **59**, no. 22, (2005)

[7] J. Cui, W. Zhai, M. K. Lu, H. Zhang, M. Pang and G. F. Yang, Optik, **208**, (2020)

[8] X. Wang, X. Ma, Q. Nie and M. Wang, Intermetallics, **31**, (2012)

[9] Y. Lei, R. Sun, J. Lei, Y. Tang and W. Opt. Lasers Eng., **48**, no. 9, (2010)

[10] P. Jiang, X. L. He, X. A. Li, L. Yu and H. Wang, Surf. Coat., **130**, no. 1, (2000)

[11] Y. Tian and C. Z. Chen, Mater. Lett., vol. **61**, no. 3, (2007)

[12] P. Ramasobane, P. M. Mashinini and B. N. Masina, Matec Web conf., (2022)

[13] L. Li, J. Wang, P. Lin and H. Liu, Ceram. Int., **43**, (2017)